Kilohertz Electrical Stimulation Nerve Conduction Block: Effects of Electrode Material

Yogi A. Patel, *Student Member, IEEE*, Brian S. Kim, and Robert J. Butera, *Senior Member, IEEE*

***Abstract*— Kilohertz electrical stimulation (KES) has enabled a novel new paradigm for spinal cord and peripheral nerve stimulation to treat a variety of neurological diseases. KES can excite or inhibit nerve activity and is used in many clinical devices today. However, the impact of different electrode materials on the efficacy of KES is unknown. We investigated the effect of different electrode materials and their respective charge injection mechanisms on KES nerve block thresholds using 20- and 40-kHz current-controlled sinusoidal KES waveforms. We evaluated the nerve block threshold and the power requirements for achieving an effective KES nerve block. In addition, we evaluated potential effects on the onset duration and recovery of normal conduction after delivery of KES. We found that thresholds and the onset and recovery of KES nerve block are not a function of the electrode material. In contrast, the power dissipation varies among electrode materials and is a function of the materials' properties at high frequencies. We conclude that materials with a proven track record of chronic stability, both for the tissue and electrode, are suitable for developing KES nerve block therapies.**

***Index Terms*— Electrical stimulation, nerve block, stimulation, neural interfaces, kilohertz high frequency alternating current, KHFAC, HFAC, KES.**

I. Introduction

KILOHERTZ electrical stimulation (KES) has garnered significant interest in the past decade for treatment of neurological disorders. KES spinal cord stimulation has been shown to treat chronic pain without significant parasthesia (Nevro Corp., Redwood City, CA, [1], [2]), while KES nerve stimulation has been demonstrated to reduce post-amputee pain (Neuros Medical Inc., Cleveland, OH, [3]) and impact weight loss in obese patients (Enteromedics Inc., St. Paul, MN, [4]). Outside the clinic, KES has been shown to induce repeatable and reversible conduction block of nerve activity [5]–[7].

The ability to block nerve activity using KES has been demonstrated in a wide range of somatic and autonomic nerves using both mammalian [5], [6], [8] and non-mammalian [9] animal models. The ability to achieve a safe, effective, and reversible block of nerve conduction is impacted by the electrode used to interface with the target tissue. Published results to date have highlighted the role of inter-pole distance [10] and electrode contact geometry [7], however we are unaware of any previous report (Table I of [7]) investigating the effect of electrode material on KES outcomes. The goal of this investigation is to understand the impact of different electrode materials with different charge injection mechanisms on KES nerve block.

Two primary charge transfer mechanisms exist at the electrode/electrolyte interface - Faradaic and non-Faradaic. Faradaic charge transfer takes place by directly transferring electrons from the electrode to the electrolyte and reducing (electron transfer from electrode to electrolyte) or oxidizing (electron transfer from electrolyte to electrode) chemical species in the electrolyte. Reversibility (or irreversibility) of the electrochemical reactions is dependent upon the electrode material, waveforms, and current densities and can be detrimental to the tissue, electrode, or both. In contrast, non-Faradaic reactions redistribute the charged electrochemical species present within the electrolyte, with no direct electron transfer into the electrolyte. Non-Faradaic reactions provide an entirely reversible charge transfer process with minimal to no tissue damage or electrode dissolution [11], [12].

Faradaic and non-Faradaic charge transfer mechanisms are often described as charge storing and charge dissipating mechanisms, respectively. These characteristics enable description of both charge transfer mechanisms with electrical circuit models represented by a parallel capacitance (non-Faradaic reactions) and resistance (Faradaic reactions). From this simple model, it can be understood that faradaic reactions mediate charge transfer with low frequencies, while non-Faradaic dominate at high frequencies. However both Faradaic and non-Faradaic mechanisms can be present when high stimulation currents are used. In addition, all real-world KES waveforms contain some level of direct current contamination, which may lead to an increase in Faradaic reactions.

Manuscript received April 22, 2017; revised June 15, 2017; accepted July 24, 2017. Date of publication August 11, 2017; date of current version January 8, 2018. This work was supported in part by the Georgia Tech TI:GER Program (YAP) and in part by NIH (subcontract to RJB) under Grant 2R01EB016407. *(Corresponding author: Yogi A. Patel.)*

Y. A. Patel is with the Bioengineering Graduate Program, Georgia Institute of Technology, Atlanta, GA 30332 USA, and also with the Department of Biomedical Engineering, Georgia Institute of Technology, Atlanta, GA 30332 USA (e-mail: yapatel@gatech.edu).

B. S. Kim is with the Department of Biomedical Engineering, Georgia Institute of Technology, Atlanta, GA 30332 USA.

R. J. Butera is with the Bioengineering Graduate Program, Georgia Institute of Technology, Atlanta, GA 30332 USA, also with the Department of Biomedical Engineering, Georgia Institute of Technology, Atlanta, GA 30332 USA, and also with the School of Electrical and Computer Engineering, Georgia Institute of Technology, Atlanta, GA 30332 USA.

Digital Object Identifier 10.1109/TNSRE.2017.2737954

We have recently studied the effect of electrode geometry on KES nerve block [7]. The focus of the present study is to experimentally evaluate the effect of different electrode materials with different charge injection mechanisms on KES nerve block power requirements. Other goals of this study are to evaluate the effects of different materials on the onset artifact duration, nerve conduction, and recovery post-KES nerve block. The electrode materials investigated in this study include Stainless Steel (SS), Platinum (Pt), Platinum-Iridium (90/10, PtIr), and Titanium Nitride (TiN), enabling evaluation of materials using Faradaic (SS), non-Faradaic (TiN), and combined Faradaic/non-Faradaic (Pt, PtIr) charge injection mechanisms.

II. Methods

A. Animal Preparation

All animal research was approved by the Georgia Institute of Technology Institutional Animal Care and Use Committee. Experiments were conducted on tibial nerves from *in vivo* urethane-anesthetized male rats (384 ± 51g, n = 12). Animals were briefly anesthetized using isoflurane in oxygen (5%, 1 liter/min flow rate) prior to delivery of urethane (IP, 1.2 g/kg in 0.9% saline). Anesthetic depth was evaluated 60 - 90 minutes post-injection by pinching the rear footpad and supplemental urethane (0.12 mg/ml) was delivered as necessary until the reflex withdrawal was eliminated. After reaching surgical depth, the animal's back was shaved from the lumbar section down to the distal end of the gastrocnemius muscle. The animal's foot was magnetically clamped to the surgical table to minimize motion during experimental trial. An incision approximately 1 - 1.5 cm in length was made along the length of the biceps femoris muscle and the sciatic nerve exposed via blunt dissection. The tibial branch of the sciatic nerve was identified and isolated from the sciatic notch down to the gastrocnemius muscle under a high magnification dissection scope. The common peroneal, sural, and collateral branches of the sciatic were cut to minimize off-target stimulation. Normal rat ringer's solution [13] was applied throughout the experiment to prevent muscle and nerve tissue dehydration. The animal's body temperature was monitored and maintained at 37 - 40 °C with a rectal temperature probe (Model BAT-12, Physitemp Instruments, Clifton, NJ) and warming pad (COM-11289, SparkFun Electronics, Niwot, CO). Preparations lasted 5 - 6 hours after which animals were euthanized via an IP injection of pentobarbital-based euthanasia drug (0.5 ml/kg, IP). All experiments were conducted at room temperature.

B. Electrophysiology Setup

The proximal end of the exposed sciatic nerve was stimulated using a bipolar cuff electrode made in-house. Two braided stainless steel wires (#793500, A-M Systems, Sequim, WA) separated by 1 mm were deinsulated and threaded through silicone tubing (#807600, A-M Systems, Sequim, WA). A second bipolar stimulation cuff electrode was placed approximately 0.2 cm distal to the block electrode in all experiments for delivery of distal test stimuli. Distal test stimuli verified that KES nerve block was localized to the site of the block electrode and did not cause neuromuscular fatigue or neurotransmitter depletion.

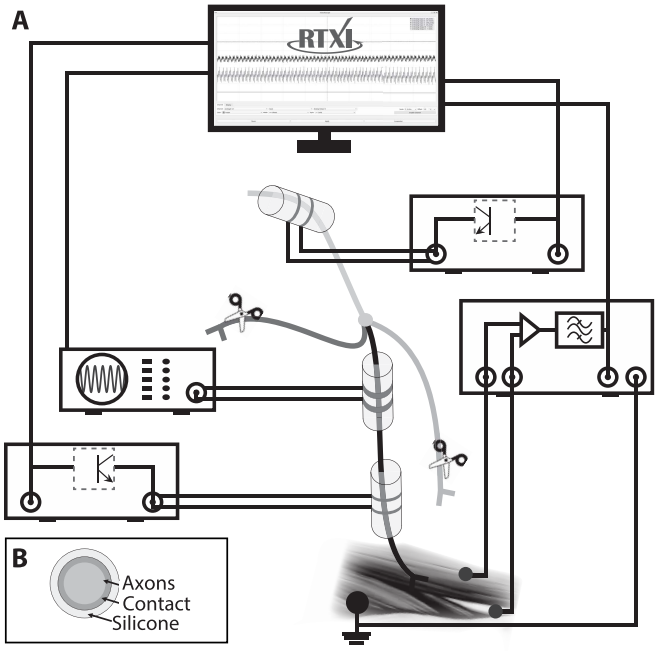

Fig. 1. Electrophysiology setup and electrode configurations. (A) The nerve was electrically stimulated at the proximal and distal ends using bipolar cuff electrodes. EMG activity was measured from the gastrocnemius muscle using intramuscular fine wire electrodes. (B) Illustration of the circumferential electrode-tissue interface. Timing and duration of stimulation events, along with measurement of activity was achieved with RTXI.

Spacing between the proximal stimulation and block electrodes was approximately 1 cm in all experiments. EMG activity was differentially measured from the gastrocnemius muscles using bipolar fine wire electrodes (Cooner Wire No. AS631, Chatsworth, CA). EMG measurements were filtered (100 - 300 Hz) and gained (1000x, Brownlee Precision Model 440, San Jose, CA) before being digitized at a rate of 20 kHz using The Real-Time eXperiment Interface (RTXI, http://www.rtxi.org, [14], [15]) with a PCI-6036E data acquisition card (National Instruments, Austin, TX). A stainless steel wire was inserted into the contralateral gastrocnemius muscle and connected to the surgical air table to electrically ground the animal, with the surgical table grounded to the amplifier (building supply ground). Figure 1A shows the complete experiment setup.

C. Electrode Fabrication

Block of the tibial nerve was achieved using SS, Pt, PtIr (90/10), TiN-Pt, and TiN-PtIr (90/10) contact pads (25.4 μm thick, ESPI Metals, Ashland, OR). Each material was evaluated in random order in each experiment. The length and width of all contacts was 2.0 mm and 0.5 mm, respectively. Electrode contact geometric surface areas (GSAs) were calculated to be 0.01 ± 0.0002 cm^2. This geometry provided complete circumferential coverage of the tibial nerve (Fig. 1B, circumference 2.0 - 2.1 mm [16]), which is critical for

minimizing the KES nerve block threshold [7]. Contacts were cut and measured under a high resolution microscope with digital calipers (measurement error = 0.01 mm), spot welded to braided (7-strand) stainless steel wire, wrapped around the nerve under a dissection microscope, and insulated using silicone (Kwik-Cast, WPI, Sarasota, FL) using previously published methods [5].

TiN coated electrodes were fabricated by adhering Pt and PtIr contacts to a 4 inch silicon wafer using parafilm tape. Leads were spot-welded to the contacts prior to TiN deposition and insulated with an additional layer of parafilm tape to prevent deposition of TiN onto lead wires. Porous TiN was sputtered (AJA Magnetron Sputter System, Scituate, MA) onto the exposed contact surfaces at a rate of 7.5 nm/min under a base pressure of 10^5 Torr and Ar and N_2 gas flow rates of 180 and 240 sccm, respectively. These parameters provided a 200 nm layer of TiN on Pt and PtIr contacts.

D. Nerve Activation and KES Block

Constant current pulses (0.3-0.5 mA_{peak}, 0.2 ms, 1 Hz) were generated using the RTXI signal generator module for proximal stimulation and an optically isolated constant current stimulator (DS3, Digitimer, Ft. Lauderdale, FL) for distal stimulation. Proximal stimulation pulses were optically-isolated using linear stimulus isolators (A395, WPI, Sarasota, FL). The KES waveform (current-controlled, continuous sinusoid) was generated using a floating current source function generator (Model 6221, Keithley Instruments, Inc, Clevelend, OH). The 2.1 mA_{peak} and 21.0 mA_{peak} ranges were used for the 20 kHz and 40 kHz KES trials, respectively. Direct current contamination of the KES waveform was randomly measured with a 10 Ω sense resistor in series with the return electrode and measured to be 150 - 500 nA. All stimulus isolation units were calibrated prior to each experiment and output offsets zeroed by visualization on an oscilloscope. Timing control of stimulation equipment was achieved by using digital I/O triggers generated from RTXI.

E. Experimental Protocols

The first trial was conducted to determine the block threshold with a given electrode and KES frequency (as previously described in [5]). The sciatic nerve was stimulated at 1 Hz using the proximal stimulation electrode to elicit supramaximal EMG activity in the gastrocnemius muscle. The block threshold was found by increasing the amplitude of the KES waveform in 0.1 mA_{peak} increments until complete block was achieved. Complete block was achieved only when the RMS voltage of the EMG measurement was equivalent to that of the measurement noise. The second trial was conducted at the empirically determined block threshold, with approximately 3 - 5 minutes between each trial. In each trial, a total of 100 stimulation pulses were delivered to the nerve (Fig. 2). The initial 21 stimulation pulses were delivered to the nerve to capture pre-KES EMG activity. KES was delivered to the nerve 150 ms after the 21st stimulation pulse at either 20 or 40 kHz with the predetermined block threshold. Test pulses were delivered to the nerve while delivery of KES

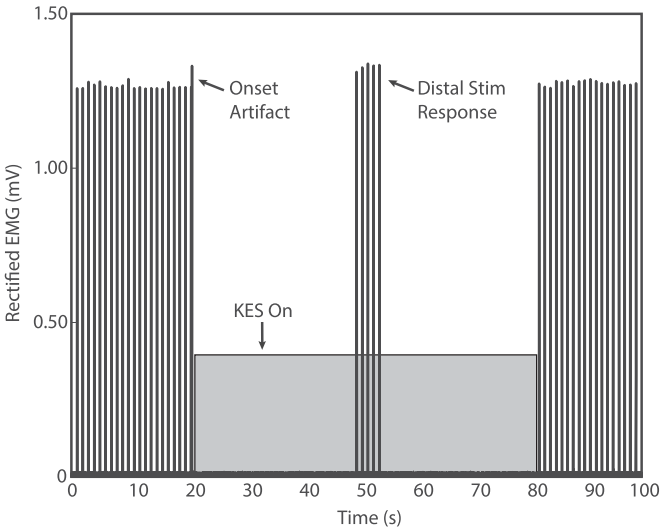

Fig. 2. Representative rectified evoked EMG data from a single trial. Each trial lasted a total of 100 seconds, with KES on for 60 seconds. Stimulation pulses were delivered via the proximal stimulation cuff electrode throughout the entire trial. Five stimulation pulses were delivered to the nerve distal to the KES electrode to assess the locality of KES nerve block.

for continuous assessment of KES nerve block efficacy. The KES waveform was automatically turned off after 60 seconds (60 stimulation pulses) with continued nerve stimulation to measure post-KES EMG activity. Figure 2 provides a pictorial description of the experimental protocol for a single trial with representative data.

F. Electrochemical Measurements

Monopolar cyclic voltammetry (CV) measurements were made for each electrode material to compute the cathodic charge storage capacity (CSC) (Fig. 3A). Measurements were made using a three electrode setup with a Ag|AgCl reference electrode and a Pt counter electrode (surface area: 0.02 cm^2). A potentiostat (VMP3, Bio-Logic) was used to sweep the potential with a scan rate of 50 mV/sec while simultaneously measuring the current flow between the working (monopolar test electrode) and counter electrodes. The potential was swept between −0.6 V and 0.8 V for SS, Pt, and PtIr electrodes and between −1.0 V and 1.0 V for TiN coated contacts. The negative current time integrals were computed for each voltammogram and averaged to obtain the mean cathodic CSC for each contact material [17].

Monopolar electrochemical impedance spectroscopy (EIS) measurements were made using the same three electrode setup to quantify frequency-dependent changes at the electrode/electrolyte interface (Fig. 3B-C). Measurements were made by sweeping a 10 mV excitation waveform over a frequency range of 1 Hz - 10^5 kHz. All electrochemical measurements were made in room temperature (25 °C) phosphate buffered saline (PBS, pH = 7.4, Sigma Aldrich, St. Louis, MO) stirred at a constant rate. The measured impedance magnitude and phase at experimentally tested KES frequencies were used for power computations. All measurements were made prior to use of electrodes in experiments.

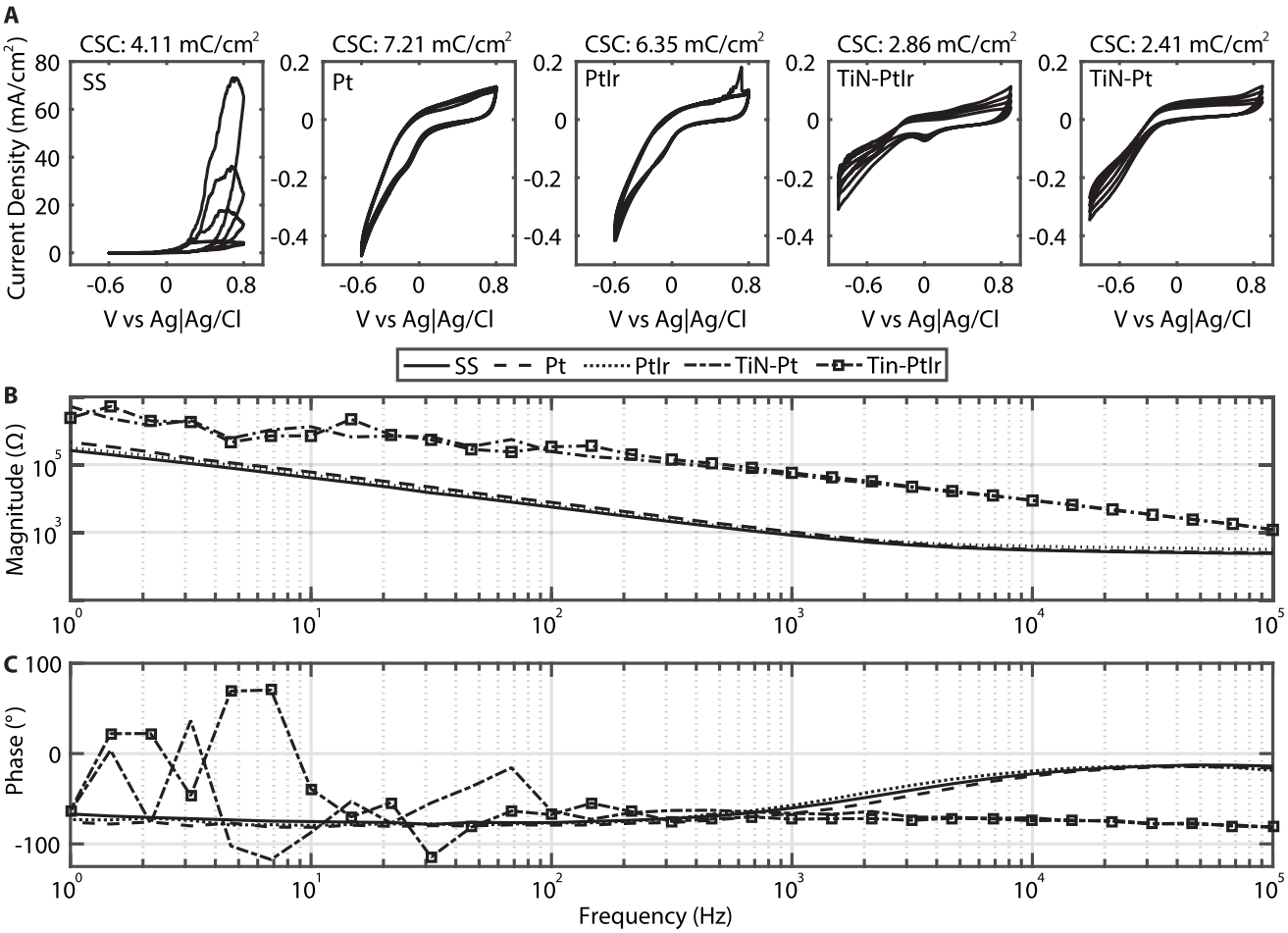

Fig. 3. Electrochemical characterization of electrodes. (A) Five voltammograms and corresponding cathodic CSC are depicted for each contact material evaluated. Cathodic CSC values shown are the average of all individual voltammograms per material. Shaded regions indicate the area used to calcaulate cathodic CSC values. (B) Representative electrochemical impedance magnitude (B) and phase angle (C) are shown for each material. Note the significant difference in the scale of the SS voltamoograms.

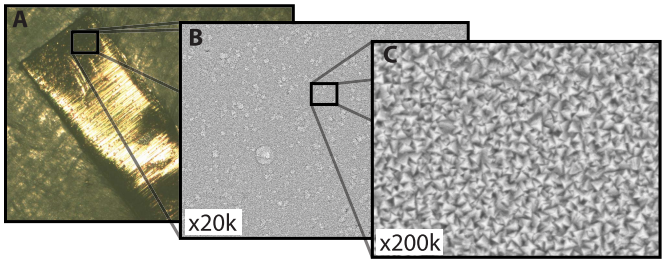

Fig. 4. Surface composition of TiN coated electrodes prior to use. (A) Light microscope image of TiN-PtIr electrode. Scanning electron microscope images (B: x20k, C: x200k) of TiN-PtIr electrode surface. Increased electrochemical surface area of TiN coating is visible.

G. Power Calculations

We used EIS magnitude, phase, and mean KES block thresholds (Fig. 5) to approximate the power required to achieve effective KES nerve conduction block with each contact material (Fig. 5B-C). The mean KES block threshold (mA_{peak}) for each contact GSA was used to generate a single cycle of a 20 and 40 kHz KES current waveform (Eqn. 1). The EIS magnitude and phase for 20 and 40 kHz were obtained by interpolating between the

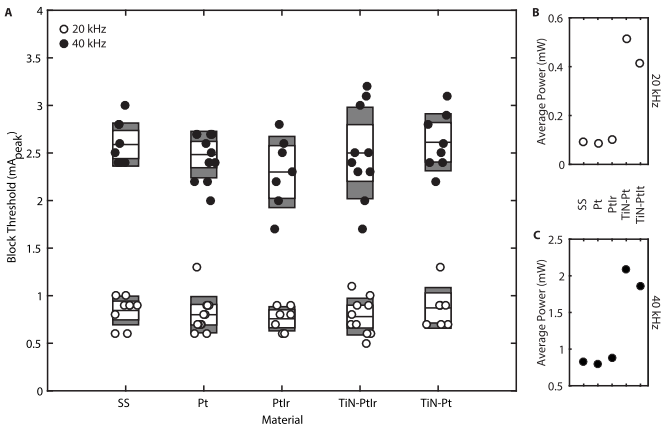

Fig. 5. (A) KES block thresholds as a function of electrode contact material for 20 and 40 kHz KES nerve block. Each dot represents an individual trial. No statistically significant difference was observed between block thresholds with a given material between 20 kHz or 40 kHz (Tukey-Kramer multiple comparison test, $\alpha = 0.05$). (B-C) Average power for each contact material computed at 20 kHz (B) and 40 kHz (C).

EIS measurements. The magnitude was used to generate an equivalent voltage waveform (Eqn. 1). The phase and generated voltage and current waveforms were then used to calculate

power (Eqn. 1).

$$\begin{aligned} I(t) &= I * sin(2 * \pi * f * t + \phi), 0 \leq t \leq T_{KES} \\ V_{RMS} &= I_{RMS} * |Z(Material, KES)| \\ Power &= V_{RMS} * I_{RMS} * cos(\phi) \end{aligned} \quad (1)$$

H. Data Analysis

All data were analyzed with MATLAB. EMG recordings were detrended and windowed (10 ms bins) to capture evoked EMG activity. The stimulus trigger was used to define the EMG window's left edge. An additional 10 ms window was used to capture baseline noise prior to stimulus delivery. The windowed data was full-wave rectified and the root mean square (RMS) voltage used as a metric for evaluating nerve and muscle activation as well as KES nerve block. The noise RMS voltage was subtracted from the EMG RMS voltage to reduce variance introduced by noise and differences in electrical coupling between experimental setups. Onset artifacts were identified by comparing the RMS voltage of a moving 10 ms window to pre-KES RMS noise values. All box plots show the population mean (center black bar), 95% confidence interval (white region), and one standard deviation (gray region).

III. Results

A. Electrochemical Characteristics of Electrodes

Electrochemical characterization of electrodes provides valuable information about the electrode stability and the response of electrodes to different stimulation waveforms. We performed CV measurements to quantify the cathodic CSC and EIS measurements to evaluate the frequency response and electrochemical reactions for each material. Figure 3A shows the cyclic voltammograms for each material evaluated.

With the exception of SS, all other electrode materials depict both Faradaic and non-Faradaic reactions as the potential is swept, with a greater Faradaic response by the Pt and PtIr electrodes and a greater non-Faradaic response displayed by the TiN electrodes. Although TiN has a high electrochemical surface area (ESA), the high sweep rate used in the CV measurements indicates a significantly lower CSC value for TiN coated electrodes compared to planar, non-coated electrodes. These conditions are a better reflection of the rate of potential change that occurs under KES applications. The voltammogram for SS depicts the presence of a developing oxide layer on the electrode surface and early stages of pitting, suggesting the onset of metal corrosion. In addition, SS presents increased water oxidation as observed by the significantly increased positive current.

The electrochemical spectra for all electrode materials are displayed in Fig. 3B-C with mean and standard deviation values at relevant KES frequencies shown in Table I. The access (or tissue) impedance for each material was taken at 100 kHz and is not subtracted from the 20 and 40 kHz impedance values. The impedance magnitude decreases across the frequency spectrum for all materials. Interestingly, although the ESA of TiN coated electrodes is greater, the impedance magnitude is significantly higher than planar, non-coated electrodes (discussed later). The decreased phase shift in the phase spectra of SS, Pt, and PtIr suggests that at high frequencies (> 1 kHz), the solution (tissue) access resistance dominates. The nearly stationary phase shift observed for TiN coated electrodes suggests the presence of a double-layer and thus non-Faradaic charge injection mechanisms throughout the entire spectrum.

TABLE I
ELECTRODE IMPEDANCE CHARACTERISTICS

Material	20 kHz	40 kHz	Access (100 kHz)
SS (Ω)	267.5 ± 89.4	249.8 ± 53.1	238.3 ± 78.6
Pt (Ω)	282.7 ± 92.4	262.0 ± 72.4	248.2 ± 36.6
PtIr (Ω)	405.3 ± 62.6	375.6 ± 53.9	349.7 ± 52.1
TiN-PtIr (Ω)	4755.1 ± 432.5	2381.8 ± 395.6	1184.2 ± 119.5
TiN-Pt (Ω)	4236.6 ± 714.1	2259.1 ± 463.7	1120.9 ± 108.3

B. Electrode Material Does Not Impact KES Nerve Block Thresholds

KES nerve block thresholds (Fig. 5) demonstrate no statistically significant dependence upon the electrode contact material at either frequency. In contrast, the average power consumption for TiN coated electrodes is higher with respect to non-coated electrodes, primarily due to the increased impedance magnitudes displayed in the EIS measurements (Fig. 3B).

C. Electrode Material Does Not Alter Post-KES Nerve Block Characteristics

The clinical utility of KES nerve block may be affected by the onset response, changes in normal nerve conduction, as well as recovery of normal conduction after KES is turned off. The onset response durations (Fig. 6) were quantified as a function of KES frequency and contact material. No statistically significant difference was observed for the onset duration as a function of electrode contact material. Quantification of pre- and post-KES evoked EMG latencies (not shown) demonstrate no difference in nerve conduction from application of 60 s of KES.

IV. Discussion

KES nerve block holds great promise as a new approach for modulating the nervous system through peripheral and autonomic nerves. Successful translation of KES nerve block therapies requires investigation of a variety of unanswered questions. The present study evaluated the effect of different electrode materials, and thus different charge injection mechanisms, on KES nerve block characteristics. Electrochemical studies were conducted to understand the charge injection mechanisms and electrical characteristics of each material. *In vivo* experiments were conducted on the rat tibial nerve with gastrocnemius muscle EMG as a readout for KES nerve block.

Our results demonstrate that KES nerve block thresholds (Fig. 5) and onset artifact duration (Fig. 6) do not

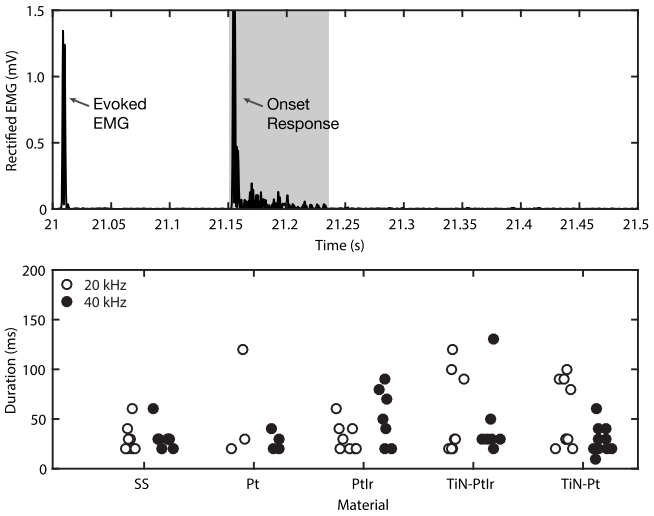

Fig. 6. Rectified EMG onset artifact and durations. (A) Rectified EMG onset artifact consists of a large, high-frequency transient spike in measured EMG activity followed by a brief period of spontaneous activation, followed by complete KES nerve block. Shaded region indicates the time window identified as the onset artifact (described in Data Anlaysis) to compute onset artifact duration for for this trial. (B) The width of the windowed rectified EMG onset artifact is used to represent the duration of the onset artifact as a function of contact material and KES frequency.

differ with different electrode materials. In contrast, the power consumption is increased by nearly 5-fold with the use of TiN-coated electrodes. These results suggest that electrode material is not a critical factor for achieving an effective KES nerve block.

Our investigation focused on 20 and 40 kHz KES sinusoidal waveforms, however the presented results are relevant to existing clinical therapies, including those that use 5 - 10 kHz because of the consistent electrochemical behavior of electrodes at all tested KES frequencies. However, many investigations suggest the use of frequencies greater than 20 kHz to achieve a true nerve conduction block, with minimal onset response and minimal sustained asynchronous activation [5], [6], [18], [19].

A typical concern with KES nerve block is the initial asynchronous activation of the nerve called the onset response. Depending on the neural circuit being modulated, the onset response can be of great concern. In somatic nerves the onset typically represents itself as activation of the muscle (and underlying sensory pathways) and can last up to 10 s, with electrode configurations demonstrated to play a critical role in minimizing the onset response [10], [20]. The onset response characterized in our investigations typically lasted <200 ms (Fig. 6). This disparity is likely due to differences in the true nerve onset measured from the nerve, lasting several milliseconds [5], versus the onset measured through force transduction, which includes many factors, such as the passive relaxation time of the muscle after being asynchronously activity.

The effects of KES nerve block (i.e, blocking of nerve activity) have been shown to persist even after cessation of KES and is commonly referred to as the carry over block effect. We did not observe this effect in our studies. The absence of the carry over block effect is likely due to the short duration (60 s) and amplitudes (at block thresholds) of KES used in our studies. This effect has been characterized as a function of the KES amplitude and duration [21] with supramaximal KES amplitudes, as opposed to at block threshold, which in our experience increases the carry over block effect duration.

The contacts used in this investigation were made of Pt or PtIr, both of which have received significant attention by the neural stimulation community [22]–[24] and are used in clinically available KES devices. Pt and PtIr utilize both faradaic and non-Faradaic charge injection mechanisms, with the contribution of each mechanism depending upon the current density and the pulse width. In the case of KES waveforms, where the pulse widths are extremely short, the non-Faradaic mechanisms dominate. The lack of a significant effect of materials on KES nerve block characteristics is likely due to the dominating electrochemical mechanisms at high frequencies. All evaluated electrode materials show a dependence upon non-Faradaic charge transfer mechanisms at KES frequencies based upon the EIS data (Fig. 3B-C).

Coating of Pt and PtIr electrodes with TiN, which has a high charge injection capacity [25], can lead to a reduction in the polarization of the electrode during stimulation and thus the power requirements for neural stimulation therapies. Our results are in contrast to this and demonstrate a higher average power when using TiN-coated electrodes for KES nerve block (Fig. 5B-C). These contrasting results are likely due to multiple factors including thickness and behavior of TiN at high frequencies. Meijs *et al.* [25] used TiN coatings 62.5-fold thicker (12.5μm) than our coatings (200 nm) to achieve substantial impedance magnitude reductions. Our attempts with thicker TiN layers were unsuccessful due to delamination and cracking of the TiN during implantation of the electrodes circumferentially around the nerve.

The fractal pattern of TiN (Fig. 4C) increases the ESA resulting in a greater number of sites for charge transfer to take place. Similar benefits are achieved with other materials and coatings, such as conducting polymer polypyrrole (PPy) doped with polystyrene sulfonate (PSS). However, utilization of the additional charge transfer sites has been shown to be frequency-dependent. Both modeling and experimental results suggest that the peaks and valleys on fractal pattern coatings are hidden from charge transfer at high frequencies [26], resembling an effective ESA closer to that of planar materials (Pt, PtIr, SS). Similar characteristics have been shown chronically *in vivo* with poly(3,4-ethylenedioxythiophene) (PEDOT) coated Michigan probes [27].

V. Conclusion

KES nerve conduction block is a powerful neuromodulation technique capable of providing fast, effective, and robust block of nerve activity. The results presented in this manuscript demonstrate the independence of KES nerve block thresholds and post-KES nerve block characteristics on various electrode materials and charge injection mechanisms. However, the material of choice can substantially

alter the power requirements based upon it's behavior at high frequencies. These results suggest that the electrode material used for KES be selected based upon proven track records of chronic stability, long-term safety, and robust manufacturing methods. For example, PtIr alloys, which primarily utilize non-Faradaic charge injection mechanisms at KES frequencies, may provide chronic stability and safety for both the nerve and electrode.

Acknowledgment

The authors thank Dr. Stuart Cogan and Atefeh Khorasgani for feedback on the manuscript and stimulating discussions on the general topic of electrode materials and electrochemical behavior at high frequencies. The authors thank Romil Modi for fabrication of TiN coated electrodes and Dr. Seung Woo Lee and Jinho Park for assistance with electrochemical measurements and feedback on the manuscript. The authors also thank Dr. Laura O'Farrell, Dr. Manfred Franke, Dr. Kip Ludwig, and Evan N. Nicolai for providing feedback and stimulating conversation on the topic of KES nerve block.

Author Contributions

YAP designed and conceived the study. BSK and YAP performed experiments. BSK, YAP, and RJB analyzed data. BSK fabricated electrodes. YAP conducted electrochemical characterization. YAP, BSK, and RJB wrote the manuscript.

References

[1] L. Kapural *et al.*, "Novel 10-kHz high-frequency therapy (HF10 therapy) is superior to traditional low-frequency spinal cord stimulation for the treatment of chronic back and leg pain: The SENZA-RCT randomized controlled trial," *Anesthesiology*, vol. 123, no. 4, pp. 851–860, 2015.

[2] M. C. Bicket, R. Y. Dunn, and S. U. Ahmed, "High-frequency spinal cord stimulation for chronic pain: Pre-clinical overview and systematic review of controlled trials," *Pain Med.*, vol. 17, no. 12, pp. 2326–2336, Dec. 2016.

[3] A. Soin, N. S. Shah, and Z.-P. Fang, "High-frequency electrical nerve block for postamputation pain: A pilot study," *Neuromodulation, Technol. Neural Interface*, vol. 18, no. 3, pp. 197–206, Apr. 2015.

[4] M. Camilleri *et al.*, "Intra-abdominal vagal blocking (VBLOC therapy): Clinical results with a new implantable medical device," *Surgery*, vol. 143, no. 6, pp. 723–731, Jun. 2008.

[5] Y. A. Patel and R. J. Butera, "Differential fiber-specific block of nerve conduction in mammalian peripheral nerves using kilohertz electrical stimulation," *J. Neurophysiol.*, vol. 113, no. 10, pp. 3923–3929, Jun. 2015.

[6] Y. A. Patel, T. Saxena, R. V. Bellamkonda, and R. J. Butera, "Kilohertz frequency nerve block enhances anti-inflammatory effects of vagus nerve stimulation," *Sci. Rep.*, vol. 7, Jan. 2017, Art. no. 39810.

[7] Y. A. Patel, B. S. Kim, W. S. Rountree, and R. J. Butera, "Kilohertz electrical stimulation nerve conduction block: Effects of electrode surface area," *IEEE Trans. Neural Syst. Rehabil. Eng.*, to be published.

[8] N. Bhadra and K. L. Kilgore, "High-frequency electrical conduction block of mammalian peripheral motor nerve," *Muscle Nerve*, vol. 32, no. 6, pp. 782–790, Dec. 2005.

[9] L. Joseph and R. J. Butera, "High-frequency stimulation selectively blocks different types of fibers in frog sciatic nerve," *IEEE Trans. Neural Syst. Rehabil. Eng.*, vol. 19, no. 5, pp. 550–557, Oct. 2011.

[10] D. M. Ackermann, N. Bhadra, E. L. Foldes, X.-F. Wang, and K. L. Kilgore, "Effect of nerve cuff electrode geometry on onset response firing in high-frequency nerve conduction block," *IEEE Trans. Neural Syst. Rehabil. Eng.*, vol. 18, no. 6, pp. 658–665, Dec. 2010.

[11] D. R. Merrill, M. Bikson, and J. G. R. Jefferys, "Electrical stimulation of excitable tissue: Design of efficacious and safe protocols," *J. Neurosci. Methods*, vol. 141, no. 2, pp. 171–198, Feb. 2005.

[12] W. M. Grill, S. E. Norman, and R. V. Bellamkonda, "Implanted neural interfaces: Biochallenges and engineered solutions," *Annu. Rev. Biomed. Eng.*, vol. 11, pp. 1–24, Jan. 2009.

[13] *Normal Rat Ringer's Solution*. Accessed: May 2016. [Online]. Available: http://cshprotocols.cshlp.org/content/2012/2/pdb.rec068312.full?textonly=true

[14] Y. A. Patel, A. George, A. D. Dorval, J. A. White, D. J. Christini, and R. J. Butera, "Hard real-time closed-loop electrophysiology with the real-time eXperiment interface (RTXI)," *PLoS Comput. Biol.*, vol. 13, no. 5, p. e1005430, 2017.

[15] R. J. Lin, J. Bettencourt, J. A. White, D. J. Christini, and R. J. Butera, "Real-time experiment interface for biological control applications," in *Proc. Annu. Int. Conf. IEEE Eng. Med. Biol. (EMBC)*, Aug. 2010, pp. 4160–4163.

[16] H. Schmalbruch, "Fiber composition of the rat sciatic nerve," *Anatomical Rec.*, vol. 215, no. 1, pp. 71–81, May 1986.

[17] S. F. Cogan, "Neural stimulation and recording electrodes," *Annu. Rev. Biomed. Eng.*, vol. 10, pp. 275–309, Aug. 2008.

[18] K. L. Kilgore and N. Bhadra, "Nerve conduction block utilising high-frequency alternating current," *Med. Biol. Eng. Comput.*, vol. 42, no. 3, pp. 394–406, May 2004.

[19] K. L. Kilgore and N. Bhadra, "Reversible nerve conduction block using kilohertz frequency alternating current," *Neuromodulation, Technol. Neural Interface*, vol. 17, no. 3, pp. 242–254, Apr. 2014.

[20] D. M. Ackermann, Jr., N. Bhadra, E. L. Foldes, and K. L. Kilgore, "Conduction block of whole nerve without onset firing using combined high frequency and direct current," *Med. Biol. Eng. Comput.*, vol. 49, no. 2, pp. 241–251, Feb. 2011.

[21] G. Yang *et al.*, "Post-stimulation block of frog sciatic nerve by high-frequency (kHz) biphasic stimulation," *Med. Biol. Eng. Comput.*, vol. 55, no. 4, pp. 585–593, Apr. 2017.

[22] S. F. Cogan, P. R. Troyk, J. Ehrlich, and T. D. Plante, "*In vitro* comparison of the charge-injection limits of activated iridium oxide (AIROF) and platinum-iridium microelectrodes," *IEEE Trans. Biomed. Eng.*, vol. 52, no. 9, pp. 1612–1614, Sep. 2005.

[23] E. K. Brunton *et al.*, "*In vivo* comparison of the charge densities required to evoke motor responses using novel annular penetrating microelectrodes," *Frontiers Neurosci.*, vol. 9, p. 265, May 2015.

[24] D. Kumsa *et al.*, "Electrical neurostimulation with imbalanced waveform mitigates dissolution of platinum electrodes," *J. Neural Eng.*, vol. 13, no. 5, p. 054001, 2016.

[25] S. Meijs, M. Fjorback, C. Jensen, and S. Sørensen, "Electrochemical properties of titanium nitride nerve stimulation electrodes: An *in vitro* and *in vivo* study," *Frontiers Neurosci.*, vol. 9, p. 268, Aug. 2015.

[26] X. Cui, J. F. Hetke, J. A. Wiler, D. J. Anderson, and D. C. Martin, "Electrochemical deposition and characterization of conducting polymer polypyrrole/PSS on multichannel neural probes," *Sens. Actuators A, Phys.*, vol. 93, no. 1, pp. 8–18, Aug. 2001.

[27] K. A. Ludwig, J. D. Uram, J. Yang, D. C. Martin, and D. R. Kipke, "Chronic neural recordings using silicon microelectrode arrays electrochemically deposited with a poly(3,4-ethylenedioxythiophene) (PEDOT) film," *J. Neural Eng.*, vol. 3, no. 1, pp. 59–70, 2006.